NASA Technical Memorandum 4180

An Experimental Study of Tip Shape Effects on the Flutter of Aft-Swept, Flat-Plate Wings

Bryan E. Dansberry, José A. Rivera, Jr.,
and Moses G. Farmer

JUNE 1990

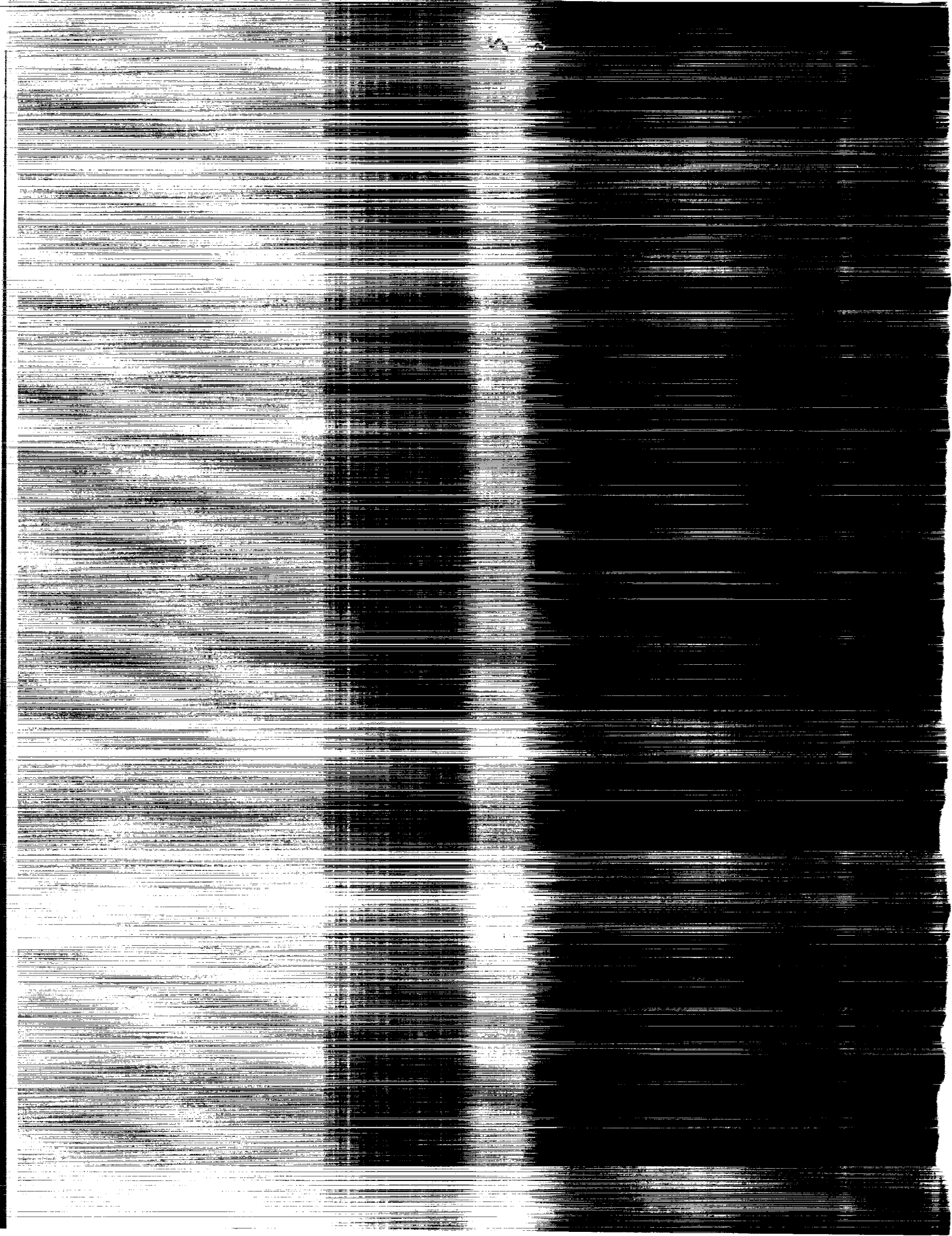

NASA Technical Memorandum 4180

An Experimental Study of Tip Shape Effects on the Flutter of Aft-Swept, Flat-Plate Wings

Bryan E. Dansberry, José A. Rivera, Jr.,
and Moses G. Farmer
Langley Research Center
Hampton, Virginia

National Aeronautics and
Space Administration
Office of Management
Scientific and Technical
Information Division

1990

Abstract

The effects of tip-chord orientation on wing flutter are investigated experimentally using six cantilever-mounted, flat-plate wing models. Experimentally determined flutter characteristics of the six models are presented for both subsonic and transonic Mach number ranges. While all models have a 60° leading-edge sweep, a 40.97° trailing-edge sweep, and a root chord of 34.75 in., they are subdivided into two series characterized by a higher aspect ratio and a lower aspect ratio. Each series is made up of three models with tip-chord orientations that are parallel to the free-stream flow, perpendicular to the model midchord line, and perpendicular to the free-stream flow. Although planform characteristics within each series of models are held constant, structural characteristics such as mode shapes and natural frequencies are allowed to vary.

Introduction

The trend toward maximizing the aerodynamic performance and structural efficiency of new airplane designs by employing new and novel aerodynamic and structural concepts may lead to unconventional geometric configurations. These configurations could have serious aeroelastic deficiencies.

Historically, parametric wind-tunnel studies such as references 1 through 5 have played a major role in increasing the understanding of flutter phenomenon so that expensive fixes to aircraft design are avoided. The present investigation was undertaken in order to obtain experimental flutter data for models with unusual tip-chord orientations. These data may be useful in assessing the importance of including flutter considerations in designing planform tip shapes.

The investigation was conducted in the Langley Transonic Dynamics Tunnel. Six flat-plate models were tested, with tip-chord orientation and aspect ratio as the primary parameters being investigated. Results are presented for two series of models: a higher aspect ratio series (H-series) and a lower aspect ratio series (L-series). Each series is made up of three models representing three tip-chord orientations: parallel to the free-stream flow (models H1 and L1), perpendicular to the model midchord line (models H2 and L2), and perpendicular to the free-stream flow (models H3 and L3). While tip-chord orientation was varied within each series, other planform variables such as leading-edge sweep, trailing-edge sweep, and root chord were held constant. Therefore, a comparison of the models within each series provides an assessment of tip-chord orientation effects. A comparison of like-numbered models in the two series shows effects due primarily to aspect ratio.

While every effort was made to hold geometric variables constant within each series, structural characteristics such as mode shapes and natural frequency were allowed to vary. It should be noted, therefore, that the results shown in this report represent integrated aerodynamic and structural effects.

Symbols

AR	full-span aspect ratio, $\frac{4B^2}{S}$
B	semispan, in.
b	reference length, in.
f_f	flutter frequency, Hz
f_n	structural frequency corresponding to nth natural mode, Hz
M	Mach number
m	calculated mass of exposed planform, slugs
q	dynamic pressure, $\frac{\rho V^2}{2}$, psf
Re	Reynolds number, $\frac{1}{\text{ft}}$
S	surface area of hypothetical full-span model, in^2
V	velocity, fps
V_f	velocity at flutter onset, fps
V_I	flutter speed index, $\frac{V_f}{b\omega_r\sqrt{\mu}}$
V_r	reference volume, ft^3
γ	ratio of specific heats
μ	mass ratio, $\frac{m}{\rho V_r}$
ρ	density of test medium, $\frac{\text{slugs}}{\text{ft}^3}$
ω_r	reference circular frequency, $\frac{1}{\text{sec}}$

Models

Physical Description

Figure 1 shows the planform geometry of the six models. All models have an identical leading-edge sweep (60°), trailing-edge sweep (40.97°), and root-chord length (34.75 in.). They are flat-plate semispan wings cut from 0.125-in-thick aluminum sheet (6061-T6). The leading edge of these models was hand filed to roughly semicircular shape, and the trailing edge and tip were left blunt. The 4.0-in. tab extending from leading to trailing edges at the root of each model was used for mounting. During testing, it was sandwiched between two angle irons to provide a cantilevered, fixed-root condition. When mounted in

the test section, a splitter plate positioned along the root chord served to isolate this mounting hardware from the free-stream flow.

The exposed planform area of models H1 through H3 was 627.5 in^2. As shown in figure 1, these model planforms differed from one another only in tip geometry. Model H1 had an aspect ratio of 2.4 and a tip chord oriented parallel to both the root chord and the free-stream flow field. Model H2 had an aspect ratio of 2.8 and a tip chord oriented perpendicular to the midchord line. Model H3 had a tip chord oriented perpendicular to the root chord and an aspect ratio of 3.1. The weight of the exposed planform area was determined by calculating the weight of the mounting tab and subtracting it from the total measured weight of each model. Since the area of each model within the H-series was the same, the calculated weight of the exposed planform area of all models within the series was a constant, 7.86 lb (0.244 slug).

Models L1 through L3 were obtained by modifying models H1, H2, and H3, respectively. The tips of these models were cut off, reducing the exposed planform area of the models by 19.2 percent to 507.1 in^2. In making these cuts, the tip orientations of models H1, H2, and H3 were preserved. The aspect ratio is 1.4 for model L1, 2.1 for model L2, and 2.5 for model L3. The weight of the exposed planform area for this series of models was 6.18 lb (0.192 slug).

Vibration Characteristics

A ground vibration test was performed on each of the models to determine their natural frequencies and node lines. First, an impact test was employed to determine the natural frequencies of the models. Then a 1-lb shaker was attached to the lower surface and used to drive the wings at each of these natural frequencies while a roving velocity probe was used to locate the node lines. The shaker was usually positioned near the wingtip along the leading edge. Potential effects of the shaker location were checked by retracing several mode shapes with the shaker attached at other locations (such as at midwing along the leading edge or at the wingtip near the trailing edge).

Table I shows the experimentally determined model natural frequencies. These frequencies were measured while the models were mounted in the test section. Sketches of the node lines corresponding to these frequencies are presented in figures 2(a) through (f). Several node lines shown in these figures terminate before reaching the wing root. In these cases, it was not possible to experimentally track the node line any further.

Flutter Experiments

Wind Tunnel

This investigation was conducted in the Langley Transonic Dynamics Tunnel (TDT). The TDT is a closed-circuit, single-return wind tunnel primarily used for aeroelastic testing. It has a slotted test section with a square cross section (with cropped corners) that measures 16 ft on a side. The TDT is a variable-density tunnel capable of operating at pressures ranging from near vacuum to atmospheric and at speeds up to Mach 1.2. Either air or R-12 can be employed as a test medium; R-12 is a heavy gas ($\gamma = 1.14$) which, at the same Mach number and dynamic pressure, results in a much higher Reynolds number than can be achieved in air. Air was used primarily for the present study with the exception of one run performed in R-12. A more detailed description of the TDT and the aeroelastic testing it is typically used for can be found in references 6 and 7.

Test Apparatus

Figure 3 shows model H1 mounted in the TDT test section. The models were mounted on a splitter-plate apparatus to place them outside the tunnel-wall boundary layer. This splitter plate was located along the root chord of the models and isolated the mounting hardware from the free-stream flow. The forward edge of the splitter plate was located 24 in. in front of the leading edge of the model. The splitter plate itself measured 76 in. streamwise and 36 in. top to bottom. The splitter plate and model were sidewall mounted to a turntable set in the test section wall, enabling test engineers to remotely adjust the model angle of attack during testing.

In order to fix the point at which the wing boundary layer became turbulent, a transition strip of number 30 grit was placed on the upper and lower surfaces of each model, 0.5 in. from the leading edge. These strips were 0.25 in. wide and extended from root to tip. Two strain-gage bridges were mounted on the surface of each model to measure root bending and torsion moments. These gages were located 2.5 in. out from the root chord along the midchord line.

Test Procedure

During flutter tests, the response of the models was visually observed by the test engineer. Outputs of the two strain-gage bridges were also monitored on a strip chart recorder. Flutter conditions were recorded when sustained or diverging oscillations were observed. A peak-hold frequency analyzer was used to identify the dominant flutter frequency

and monitor wing response as flutter conditions were approached. The mean strain-gage output was displayed on a separate strip chart channel and used as a measure of the static aerodynamic rolling moment on the model. This moment was kept to a near zero lift condition by adjusting the angle of attack of the model during the tests.

Figure 4 illustrates schematically how the flutter boundaries were defined. Tests began at a reduced total pressure so that Mach number and dynamic pressure were well below expected flutter conditions. A series of "passes" through the tunnel envelope, shown by the lines in the figure, were then made. These passes consisted of slowly increasing Mach number and dynamic pressure by increasing the tunnel motor speed until flutter was encountered or the motor limit was reached. At the end of each pass, after a flutter point had been identified or the motor limit had been reached, tunnel motor speed was reduced; air (or R-12) was then bled into the tunnel to raise the density of the test medium (thereby increasing the dynamic pressure corresponding to a given Mach number) and a new pass commenced. This process was repeated until the flutter boundary was defined.

It should be noted that only the portion of the flutter boundary ranging from the subsonic region to the minimum point of the transonic dip is determined when using this procedure. No attempt was made to define the supersonic side of the transonic dip for any of the models tested in this investigation.

Results and Discussion

A tabulation of the data obtained in this investigation is presented in table II. Flutter results of the tests performed in air are shown graphically in figures 5 and 6. In these figures, the flutter frequency and dynamic pressure are plotted against Mach number. The flutter frequency of all models was between the first and second fundamental frequencies. For all models, the flutter frequency decreased in value as Mach number increased. In the Mach number versus dynamic pressure portion of the plots, the dashed lines with symbols at both ends represent the last "pass" where flutter was not encountered. This information is included to further define the bottom of the transonic dip.

It can be seen in figure 5 that the flutter boundaries of the H-series models are grouped closely together and are similar in character. The flutter boundaries of the L-series models, shown in figure 6, are more separated than those of the H-series. This may result from the larger differences in aspect ratio and geometry within the lower aspect ratio models (the L-series) than for the higher aspect ratio models (the H-series), where the tip geometry changes affect a smaller portion of the wing. In the subsonic region, flutter boundaries for the L-series models are much higher than those for the H-series. However, the L-series models show a more pronounced transonic dip than the H-series show.

It should also be noted that for all six models the bottom of the transonic dip occurs above a Mach number of 1.0. Other highly swept models having flutter boundaries with transonic dips at similar Mach numbers can be found in references 8 and 9.

Although figure 5 shows that the flutter boundary of models H1 and H3 are almost identical, model H2, with a tip orientation perpendicular to the midchord line, has a lower flutter boundary than the models with other tip orientations. As shown in figure 6, this result held true for the L-series as well; the flutter boundary of model L2, which has a tip-chord orientation identical to model H2, is lower than those of models L1 and L3.

Figures 7 and 8 show the flutter boundaries of the six models as variations of Mach number with the nondimensional parameter flutter speed index. In the parameter flutter speed index, velocity at flutter onset is nondimensionalized using a reference length, a reference circular frequency, and mass ratio. For moderately swept and tapered planforms, the determination of a reference length is straightforward. Historically, either the semichord at the 3/4-span location or the root semichord is used. For tapered wing planforms, the root semichord may not be a representative chord. Also, for models L2 and L3 the 3/4-span station is located in the tip geometry region. Selection of the semichord at this span station would be inappropriate for these models. For the data shown in figure 7, the authors chose to use the semichord at the 3/4-span location of model H1 as the reference length for all the H-series models. Likewise, in figure 8 the semichord at the 3/4-span location of model L1 is used as the reference length for all the L-series models.

The circular frequency corresponding to the first torsion mode is commonly used as the reference frequency in calculating V_I. Unfortunately, for highly swept and tapered wings the bending and torsion modes are coupled such that determination of the first predominantly torsional mode is often difficult. For the L-series of models, the second structural mode was used as the reference frequency. Careful examination of the node line sketches in figure 2 will show that the choice of the second structural mode for the L-series was reasonably straightforward. The choice of the reference frequency for the H-series was less obvious. In this series, the second and third structural modes both show significant torsional

characteristics. However, the third structural mode was considered by the authors to be the first mode predominantly torsional in nature. For this series of models, therefore, the circular frequency corresponding to the third mode was used as the reference frequency.

In calculating the mass ratio term for models H1 and L1, the reference volume used was the volume of a conical frustum having a base diameter equal to the root chord, a height equal to the wingsemispan, and a top diameter equal to the model tip length. For the other models, the reference volume consisted of the volume of a conical frustum, generated in the same manner as for models H1 and L1, added to the volume of a cone. For these models, the local wing chord corresponding to the break in the trailing edge was used as the top diameter of the conical frustum and as the base diameter of the cone. The span station at which the break in the trailing edge occurs was used as the height of the conical frustum. The height of the cone was generated by subtracting this span station from the total span of the model. The value of mass ratio varied from near 400 for the H-series models (200 for the L-series) in the transonic region, to under 20 (both series) at the lowest Mach numbers.

Model H1 was tested in both air and R-12 to determine the effects of mass ratio and Reynolds number. Figure 9 shows the air and R-12 test results for model H1 in both dimensional and nondimensional form. These boundaries are nearly identical subsonically, with only a slight difference in the transonic dip, even though Reynolds number and mass ratio varied substantially from air to R-12 (see table II). It is possible that the small differences in the air and R-12 boundaries in the transonic region are mass ratio effects; at these Mach numbers, however, the mass ratio term is at its highest value, whereas mass ratio effects usually occur when this value is very low.

Concluding Remarks

A preliminary experimental study was performed which attempted to define the integrated aerodynamic and structural effects of tip geometry on flat-plate wing flutter. Results were shown for three tip-chord orientations: parallel to the free-stream flow, perpendicular to the model midchord line, and perpendicular to the free-stream flow. While tip-chord orientation was varied, other planform variables such as leading-edge sweep, trailing-edge sweep, root chord, and wing area were held constant. However, the dynamic characteristics of the models (i.e., mode shapes and natural frequencies) were allowed to vary. For each tip-chord orientation, flutter boundaries were defined for two models, each representing a different aspect ratio.

While the flutter boundaries of the higher aspect ratio model were very similar in character, those of the lower aspect ratio series showed more effect of tip shape, particularly in the transonic region. For models of identical tip-chord orientation, the reduction in aspect ratio resulted in a large increase in flutter dynamic pressure in the subsonic region. However, in the transonic region the reduction in aspect ratio produced boundaries with a pronounced transonic dip, resulting in a much smaller gain in flutter dynamic pressure than was seen in the subsonic region.

Compared with the other orientations tested, a tip chord oriented perpendicular to the wing midchord line appeared to reduce the flutter dynamic pressure by a modest amount.

NASA Langley Research Center
Hampton, VA 23665-5225
March 29, 1990

References

1. Theodorsen, Theodore; and Garrick, I. E.: *Mechanism of Flutter—A Theoretical and Experimental Investigation of the Flutter Problem.* NACA Rep. 685, 1940.
2. Barmby, J. G.; Cunningham, H. J.; and Garrick, I. E.: *Study of Effects of Sweep on the Flutter of Cantilever Wings.* NACA Rep. 1014, 1951. (Supersedes NACA TN 2121.)
3. Unangst, John R.; and Jones, George W., Jr.: *Some Effects of Sweep and Aspect Ratio on the Transonic Flutter Characteristics of a Series of Thin Cantilever Wings Having a Taper Ratio of 0.6.* NASA TN D-1594, 1963. (Supersedes NACA RM L55I13a and NACA RM L53G10a.)
4. Doggett, Robert V., Jr.; and Soistmann, David L.: *Some Low-Speed Flutter Characteristics of Simple Low-Aspect-Ratio Delta Wing Models.* NASA TM-101547, 1989.
5. *Flutter Criteria for Preliminary Design.* Final Eng. Rep. 2-53450/3R467 (Contract NOw 61-1072c), Aeronautics and Missiles Div., Chance Vought Corp., Sept. 1963. (Available from DTIC as AD 346 962.)
6. Reed, Wilmer H., III: *Aeroelasticity Matters: Some Reflections on Two Decades of Testing in the NASA Langley Transonic Dynamics Tunnel.* NASA TM-83210, 1981.
7. Ricketts, Rodney H.: *Selected Topics in Experimental Aeroelasticity at the NASA Langley Research Center.* NASA TM-86436, 1985.
8. Durham, Michael H.; Cole, Stanley R.; Cazier, F. W., Jr.; Keller, Donald F.; Parker, Ellen C.; and Wilkie, W. Keats: *Experimental Transonic Flutter Characteristics of Supersonic Cruise Configurations.* NASA TM-102638, 1990.
9. Nakai, Eiichi; Morita, Toshiyuki; Kikuchi, Takao; Takahashi, Minoru; and Tookubo, Masatoshi: *Transonic and Supersonic Flutter Characteristics of Low Aspect Ratio and Sweptback Thin Cantilever Wings.* NAL TR-288, National Aerospace Lab., 1972.

Table I. First Five Measured Natural Frequencies

	Frequency, Hz, for model—					
	H1	H2	H3	L1	L2	L3
f_1	4.4	4.1	4.1	8.0	8.1	7.8
f_2	16.7	17.1	17.4	23.0	25.0	27.8
f_3	28.8	27.2	26.4	51.0	44.1	40.5
f_4	40.0	42.0	42.8	54.2	62.5	61.1
f_5	62.4	63.6	61.2	87.1	99.6	97.4

Table II. Summary of Data

M	q, psf	V_f, ft/sec	ρ, $\frac{\text{slugs}}{\text{ft}^3}$	Re, $\frac{1}{\text{ft}}$	f_f, Hz	$\frac{f_f}{f_2}$	V_r, ft^3	m, slugs	μ	ω_r, 1/sec	b, in.	V_I
Model H1 (air)												
1.05	49.7	1094.3	0.000083	0.27×10^6			7.120	0.244	412.9	181.0	8.52	0.419
.99	54.6	1034.7	.000102	.31	8.2	0.491	7.120	.244	336.0	181.0	8.52	.439
.92	64.6	974.7	.000136	.38	9.4	.563	7.120	.244	252.0	181.0	8.52	.478
.85	69.3	913.8	.000166	.43	10.4	.623	7.120	.244	206.4	181.0	8.52	.495
.71	72.4	778.4	.000239	.51	11.9	.713	7.120	.244	143.4	181.0	8.52	.506
.57	74.4	630.8	.000374	.63	12.3	.737	7.120	.244	91.6	181.0	8.52	.513
.42	75.0	476.0	.000662	.81	12.5	.749	7.120	.244	51.8	181.0	8.52	.515
.23	73.7	257.0	.002232	1.50	13.2	.790	7.120	.244	15.4	181.0	8.52	.510
Model H1 (R-12)												
1.06	56.8	520.1	0.000420	0.85×10^6	8.3	0.497	7.120	0.244	81.6	181.0	8.52	0.448
.98	59.5	481.2	.000514	.96	9.1	.545	7.120	.244	66.7	181.0	8.52	.458
.93	64.8	459.1	.000615	1.09	9.3	.557	7.120	.244	55.7	181.0	8.52	.479
.86	68.2	425.9	.000752	1.24	10.2	.611	7.120	.244	45.6	181.0	8.52	.491
.72	73.7	356.9	.001157	1.58	11.6	.695	7.120	.244	29.6	181.0	8.52	.510
.58	74.9	287.0	.001819	1.99	12.2	.731	7.120	.244	18.8	181.0	8.52	.515
.43	76.7	217.0	.003258	2.69	12.7	.760	7.120	.244	10.5	181.0	8.52	.521
Model H2 (air)												
1.03	44.3	1072.7	0.000077	0.25×10^6	8.0	0.468	7.066	0.244	448.5	170.9	8.52	0.417
.97	53.6	1020.2	.000103	.31	9.0	.526	7.066	.244	335.3	170.9	8.52	.459
.87	62.8	930.7	.000145	.38	10.3	.602	7.066	.244	238.1	170.9	8.52	.497
.80	66.4	866.2	.000177	.43	11.0	.643	7.066	.244	195.1	170.9	8.52	.511
.68	67.8	750.1	.000241	.50	12.1	.708	7.066	.244	143.3	170.9	8.52	.516
.55	68.5	607.7	.000371	.61	12.6	.737	7.066	.244	93.1	170.9	8.52	.519
.40	69.1	452.2	.000676	.78	13.1	.766	7.066	.244	51.1	170.9	8.52	.521
.22	68.4	244.0	.002298	1.48	13.6	.795	7.066	.244	15.0	170.9	8.52	.519
Model H3 (air)												
1.06	49.3	1110.2	0.000080	0.26×10^6	8.5	0.489	7.021	0.244	434.4	165.9	8.52	0.452
.99	53.5	1055.7	.000096	.29	8.9	.511	7.021	.244	362.0	165.9	8.52	.471
.92	64.5	992.3	.000131	.37	10.3	.592	7.021	.244	265.3	165.9	8.52	.517
.84	69.4	914.4	.000166	.42	11.1	.638	7.021	.244	209.4	165.9	8.52	.536
.72	72.9	799.7	.000228	.50	12.8	.736	7.021	.244	152.4	165.9	8.52	.550
.58	75.2	652.7	.000353	.61	12.9	.741	7.021	.244	98.5	165.9	8.52	.558

Table II. Concluded

M	q, psf	V_f, ft/sec	ρ, $\frac{\text{slugs}}{\text{ft}^3}$	Re, $\frac{1}{\text{ft}}$	f_f, Hz	$\frac{f_f}{f_2}$	V_r, ft^3	m, slugs	μ	ω_r, 1/sec	b, in.	V_I
Model L1 (air)												
1.05	107.2	1103.7	0.000176	0.57×10^6	11.9	0.517	6.302	0.192	173.1	144.5	11.17	0.624
1.02	113.8	1083.1	.000194	.61	12.2	.530	6.302	.192	157.0	144.5	11.17	.643
1.00	122.3	1064.1	.000216	.66	12.6	.548	6.302	.192	141.0	144.5	11.17	.666
.98	130.2	1050.4	.000236	.71	13.5	.587	6.302	.192	129.1	144.5	11.17	.687
.91	145.0						6.302	.192		144.5	11.17	
.85	149.3	930.3	.000345	.88	17.0	.739	6.302	.192	88.3	144.5	11.17	.736
.78	149.2	861.6	.000402	.94	17.4	.757	6.302	.192	75.8	144.5	11.17	.736
.70	149.5	780.4	.000491	1.03	17.8	.774	6.302	.192	62.0	144.5	11.17	.737
.56	147.3	631.8	.000738	1.23	18.4	.800	6.302	.192	41.3	144.5	11.17	.731
.50	147.4	560.9	.000937	1.37	18.5	.804	6.302	.192	32.5	144.5	11.17	.731
.36	138.6	409.0	.001657	1.76	19.2	.835	6.302	.192	18.4	144.5	11.17	.709
.32	137.3	358.0	.002143	1.99	19.4	.843	6.302	.192	14.2	144.5	11.17	.706
Model L2 (air)												
1.05	51.9	1092.3	0.000087	0.28×10^6	11.0	0.440	6.050	0.192	364.8	157.1	11.17	0.391
1.02	58.1	1067.3	.000102	.32	11.3	.452	6.050	.192	311.1	157.1	11.17	.414
1.00	66.3	1051.2	.000120	.37	11.9	.476	6.050	.192	264.5	157.1	11.17	.442
.97	78.8	1031.9	.000148	.44	12.8	.512	6.050	.192	214.4	157.1	11.17	.482
.96	89.6	1023.7	.000171	.50	13.5	.540	6.050	.192	185.6	157.1	11.17	.514
.94	100.5	1007.5	.000198	.57	14.5	.580	6.050	.192	160.3	157.1	11.17	.544
.91	108.0	982.0	.000224	.62	15.1	.604	6.050	.192	141.7	157.1	11.17	.564
.89	116.0	965.3	.000249	.67	15.8	.632	6.050	.192	127.5	157.1	11.17	.584
.85	119.5	927.2	.000278	.72	16.3	.652	6.050	.192	114.2	157.1	11.17	.593
.81	124.6	889.4	.000315	.77	17.4	.696	6.050	.192	100.7	157.1	11.17	.606
.70	128.2	778.6	.000423	.88	18.3	.732	6.050	.192	75.0	157.1	11.17	.615
.58	128.4	653.1	.000602	1.04	19.2	.768	6.050	.192	52.7	157.1	11.17	.615
.46	129.4	532.1	.000914	1.24	20.1	.804	6.050	.192	34.7	157.1	11.17	.618
.33	118.8				20.7	.828	6.050	.192		157.1	11.17	
.29	114.5	328.0	.002129	1.80	20.7	.828	6.050	.192	14.9	157.1	11.17	.581
Model L3 (air)												
1.03	82.2	1076.0	0.000142	0.45×10^6	12.8	0.460	5.867	0.192	230.5	174.7	11.17	0.436
.98	85.2	1038.5	.000158	.48	12.8	.460	5.867	.192	207.1	174.7	11.17	.444
.98	91.2	1042.0	.000168	.50	13.2	.475	5.867	.192	194.8	174.7	11.17	.459
.97	98.5	1034.7	.000184	.54	13.6	.489	5.867	.192	177.9	174.7	11.17	.477
.96	105.3	1028.7	.000199	.59	14.0	.504	5.867	.192	164.4	174.7	11.17	.493
.95	113.3	1019.5	.000218	.63	14.8	.532	5.867	.192	150.1	174.7	11.17	.512
.94	122.6	1008.7	.000241	.69	15.6	.561	5.867	.192	135.8	174.7	11.17	.532
.91	130.6	983.6	.000270	.75	16.4	.590	5.867	.192	121.2	174.7	11.17	.549
.88	138.5	953.0	.000305	.81	16.8	.604	5.867	.192	107.3	174.7	11.17	.566
.83	143.1	905.6	.000349	.87	18.0	.647	5.867	.192	93.8	174.7	11.17	.575
.78	148.7	856.9	.000405	.95	18.8	.676	5.867	.192	80.8	174.7	11.17	.586
.71	151.2	789.6	.000485	1.03	20.4	.734	5.867	.192	67.5	174.7	11.17	.591
.64	151.5				20.8	.748	5.867	.192		174.7	11.17	
.51	154.2	580.9	.000914	1.39	21.6	.777	5.867	.192	35.8	174.7	11.17	.597
.37	151.0	421.0	.001704	1.86	22.8	.820	5.867	.192	19.2	174.7	11.17	.591

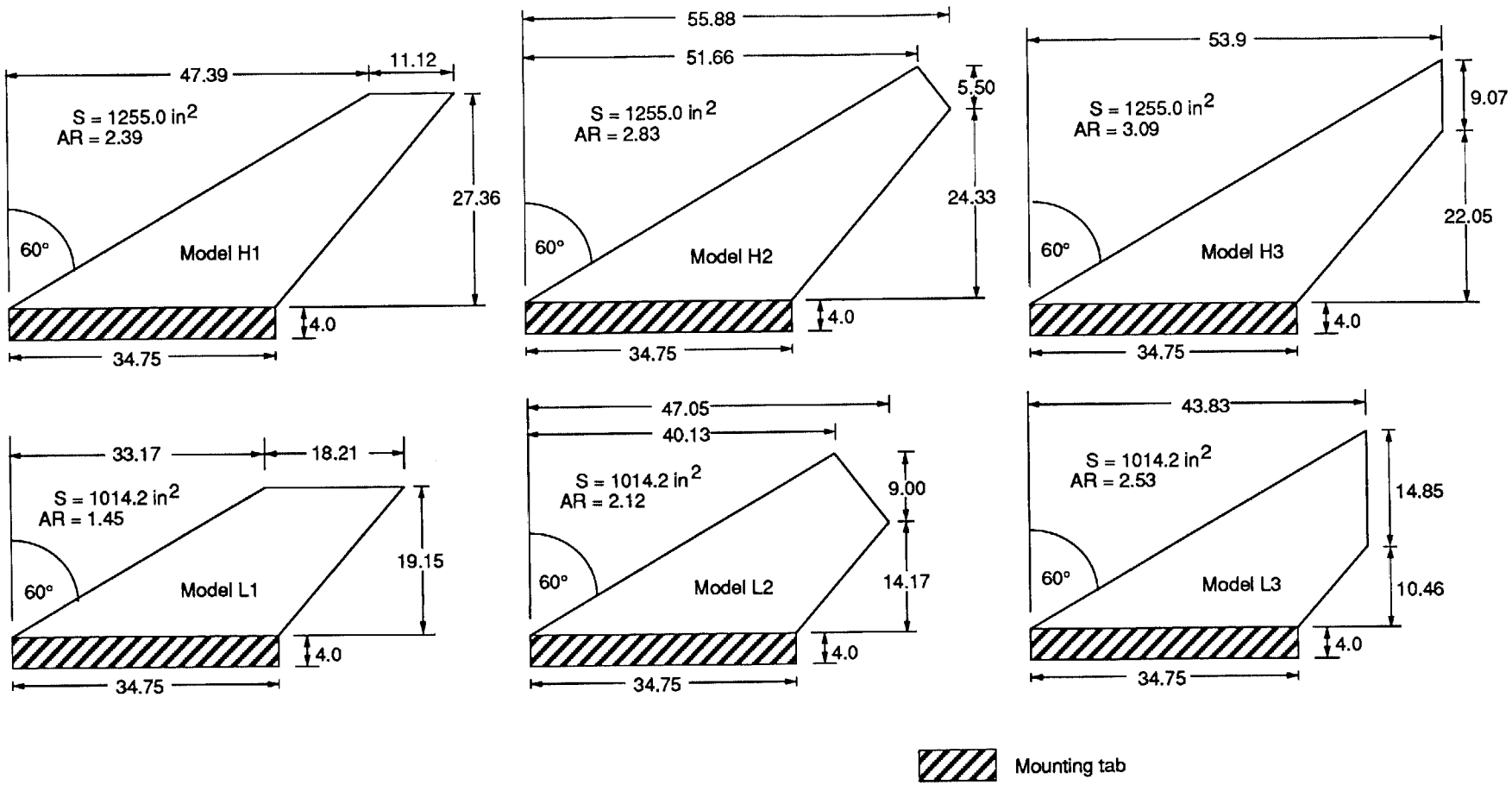

Figure 1. Planform geometry of flat-plate models. Dimensions in inches.

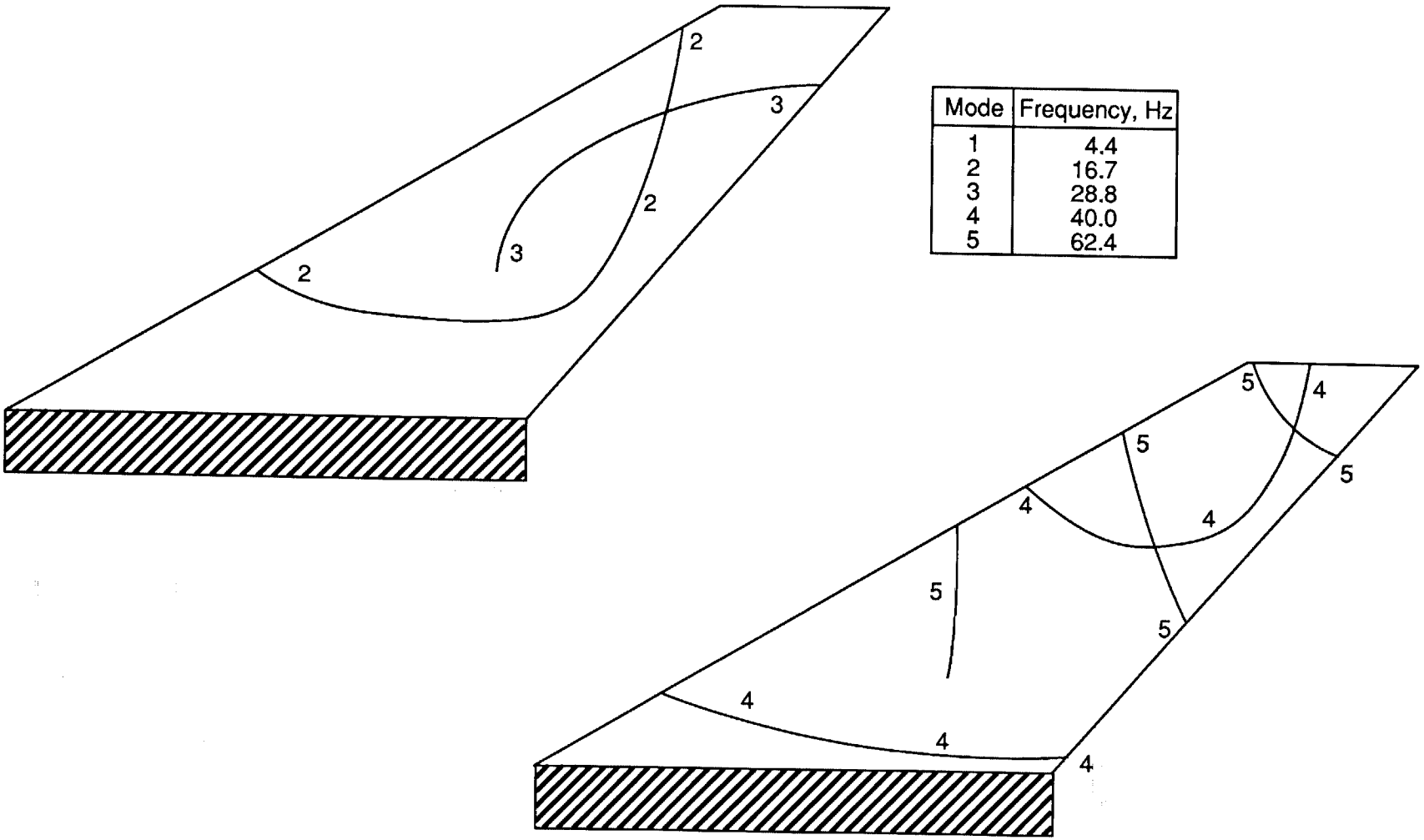

Mode	Frequency, Hz
1	4.4
2	16.7
3	28.8
4	40.0
5	62.4

(a) Model H1.

Figure 2. Measured node lines of models.

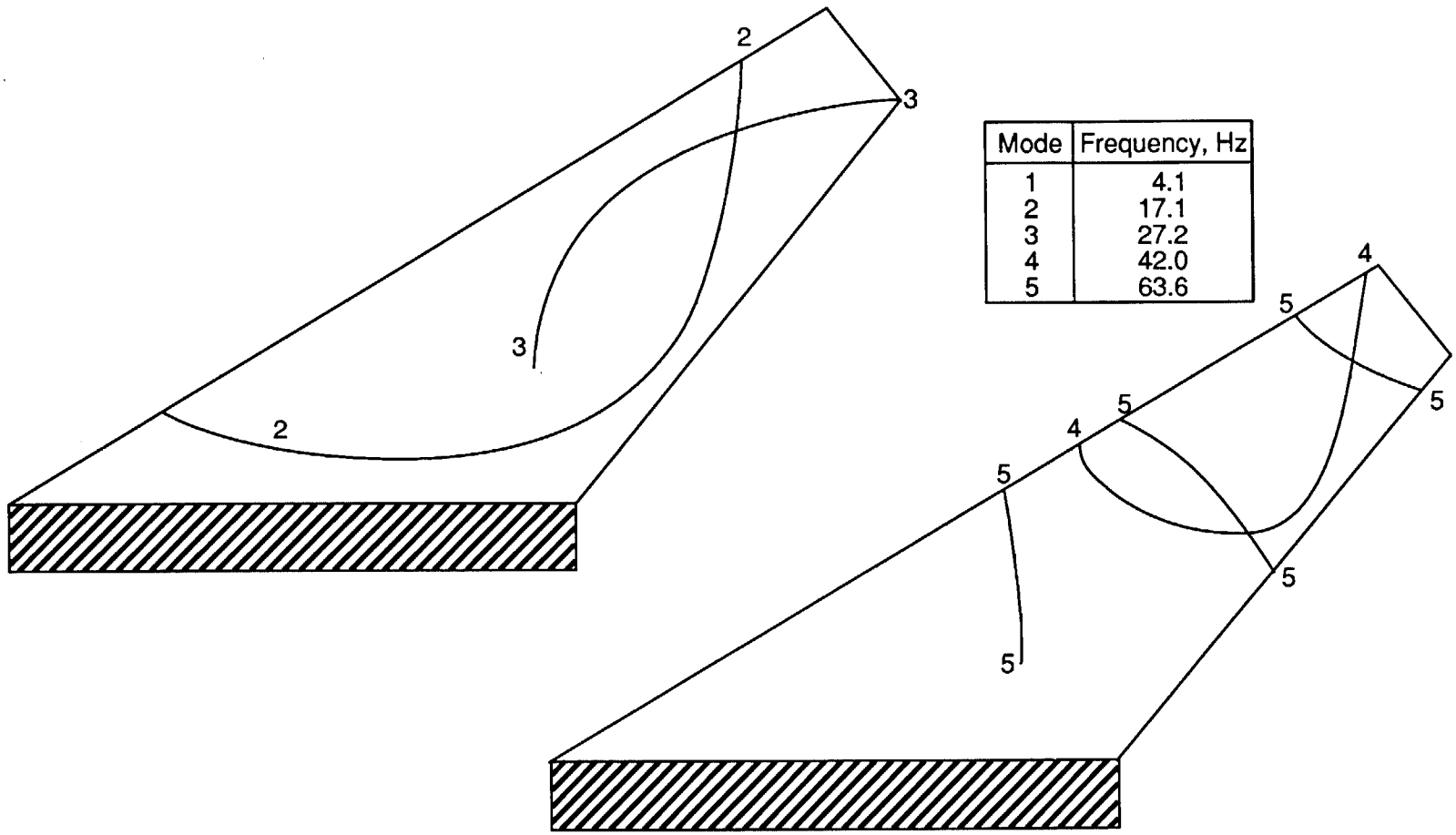

Mode	Frequency, Hz
1	4.1
2	17.1
3	27.2
4	42.0
5	63.6

(b) Model H2.

Figure 2. Continued.

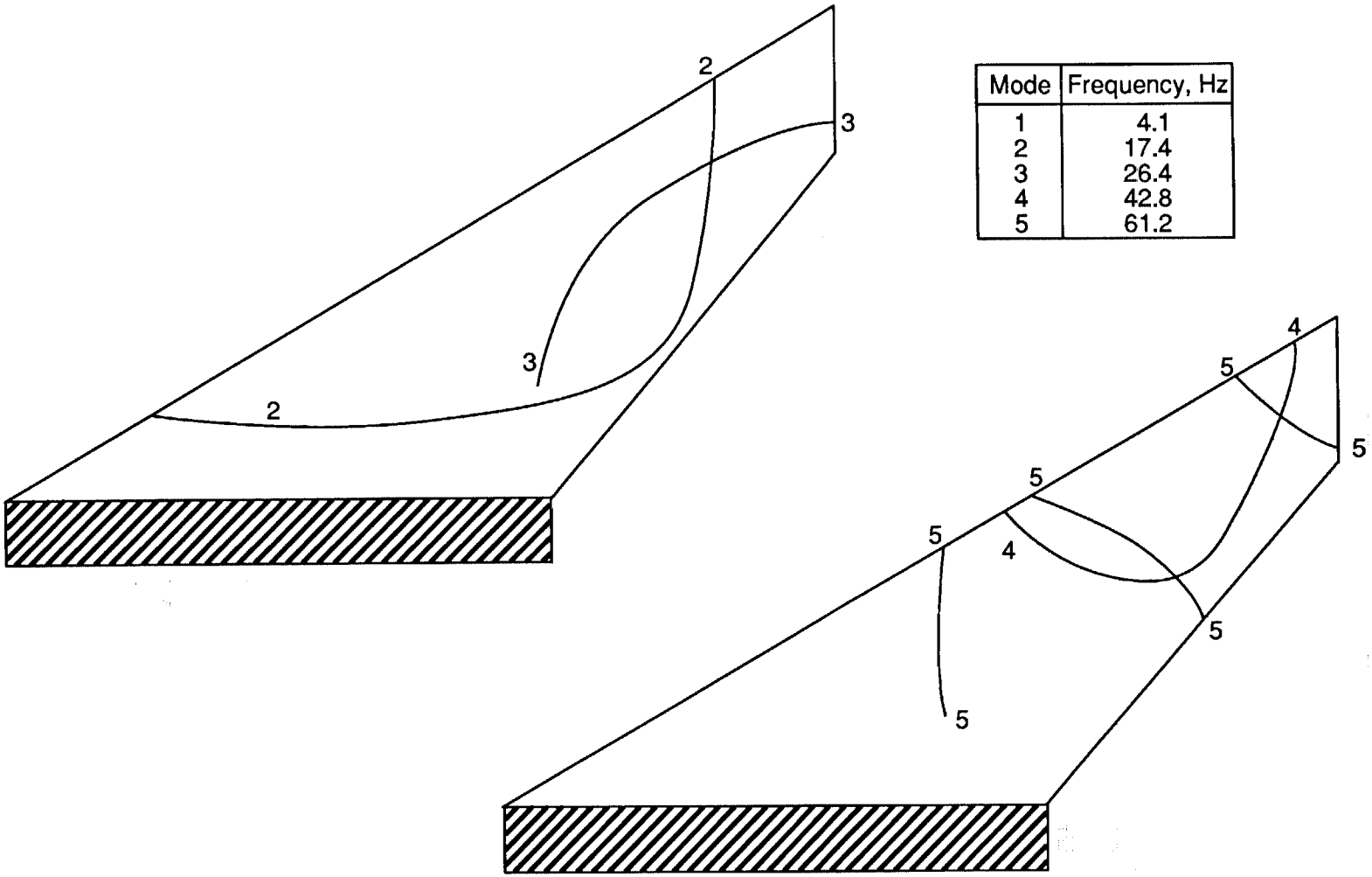

Mode	Frequency, Hz
1	4.1
2	17.4
3	26.4
4	42.8
5	61.2

(c) Model H3.

Figure 2. Continued.

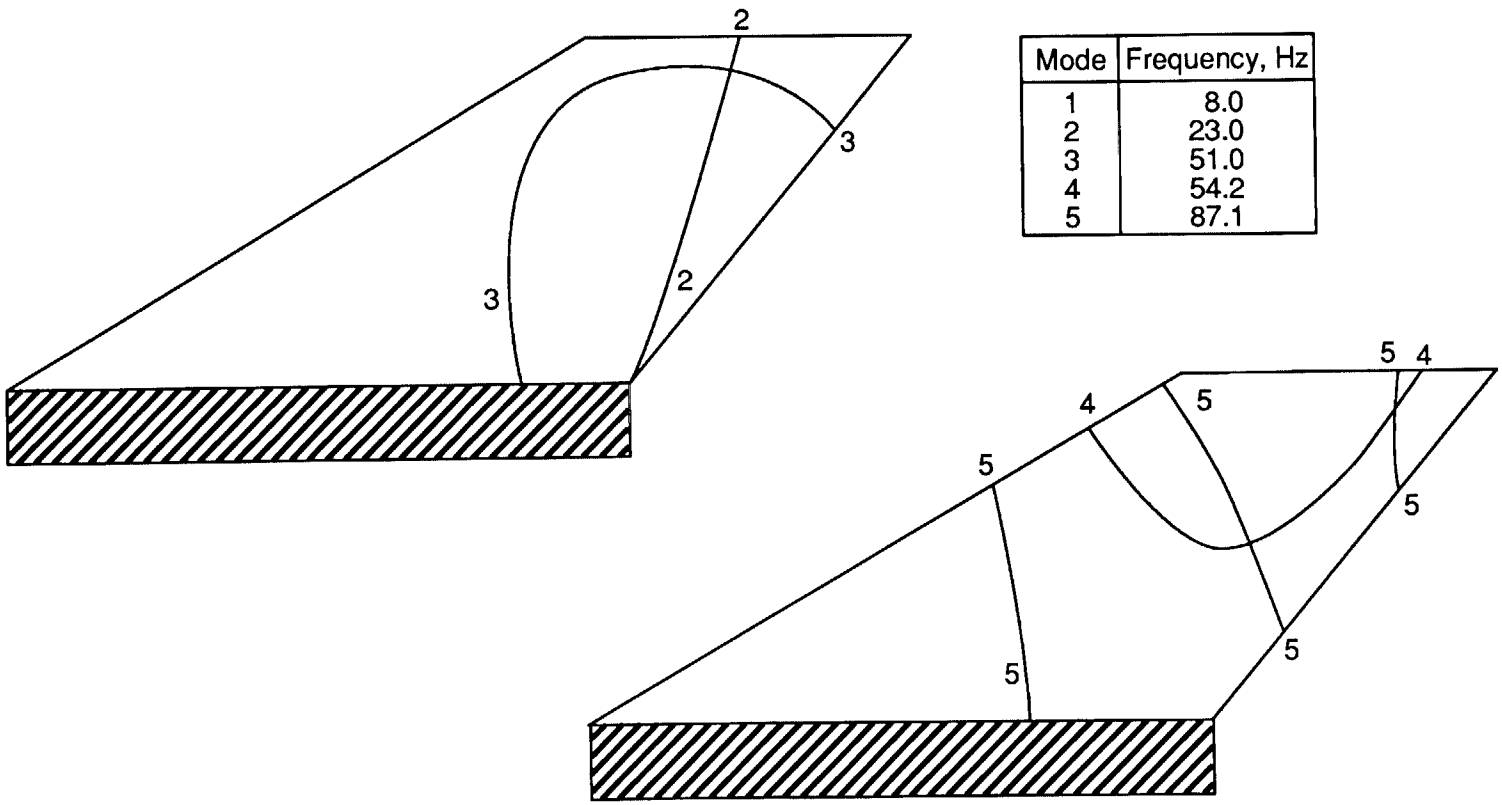

Mode	Frequency, Hz
1	8.0
2	23.0
3	51.0
4	54.2
5	87.1

(d) Model L1.

Figure 2. Continued.

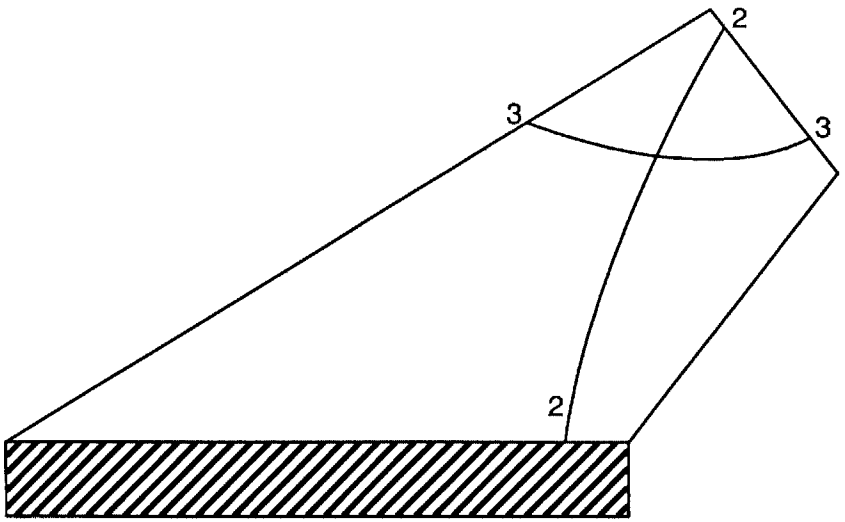

Mode	Frequency, Hz
1	8.1
2	25.0
3	44.1
4	62.5
5	99.6

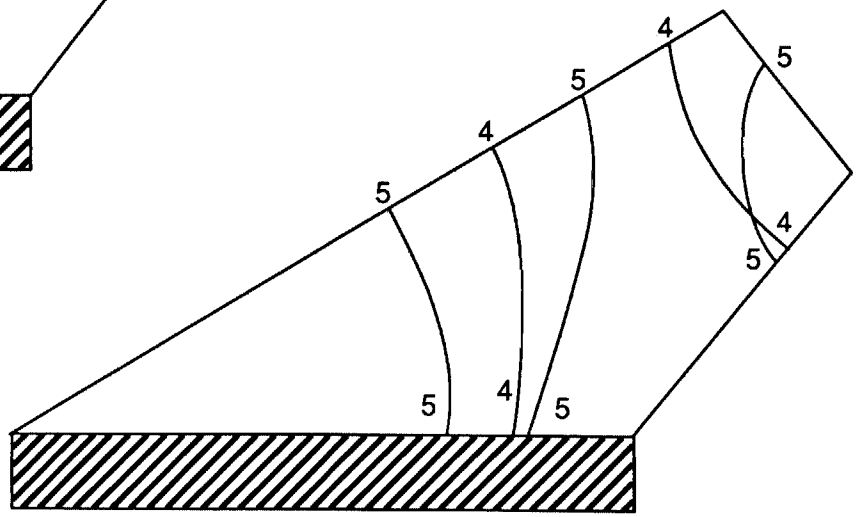

(e) Model L2.

Figure 2. Continued.

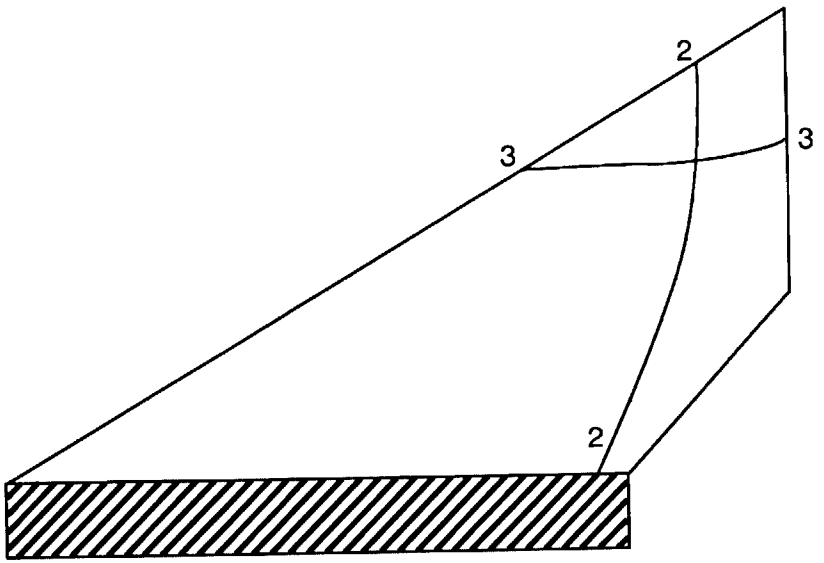

Mode	Frequency, Hz
1	7.8
2	27.8
3	40.5
4	61.1
5	97.4

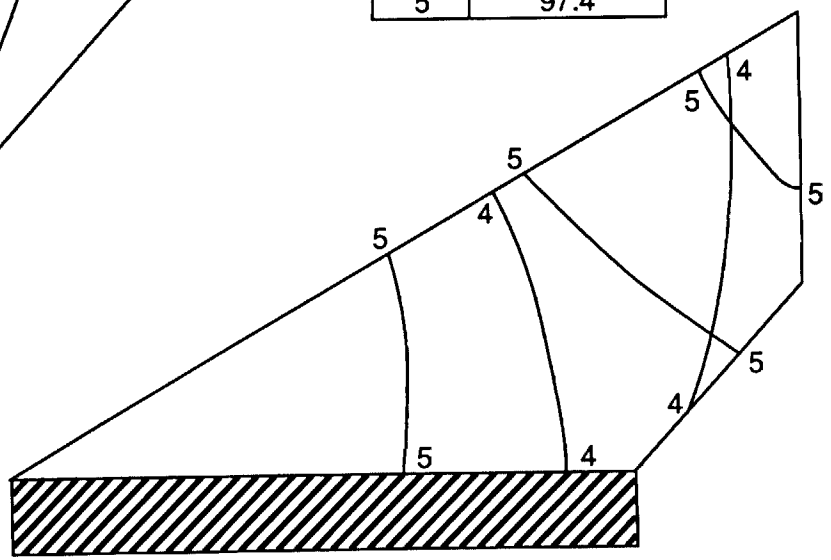

(f) Model L3.

Figure 2. Concluded.

L-89-5237

Figure 3. Model H1 mounted in TDT test section.

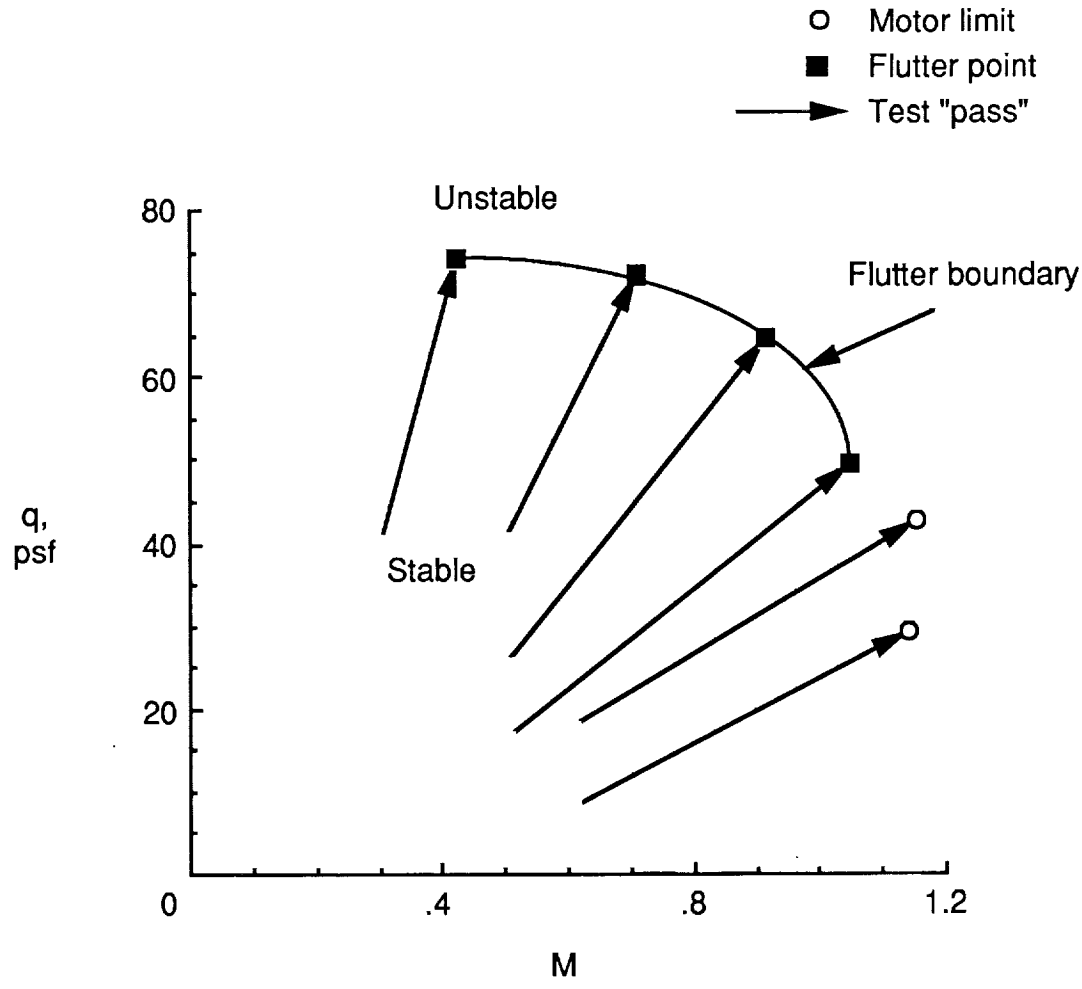

Figure 4. Test procedure used in TDT to determine typical flutter boundary.

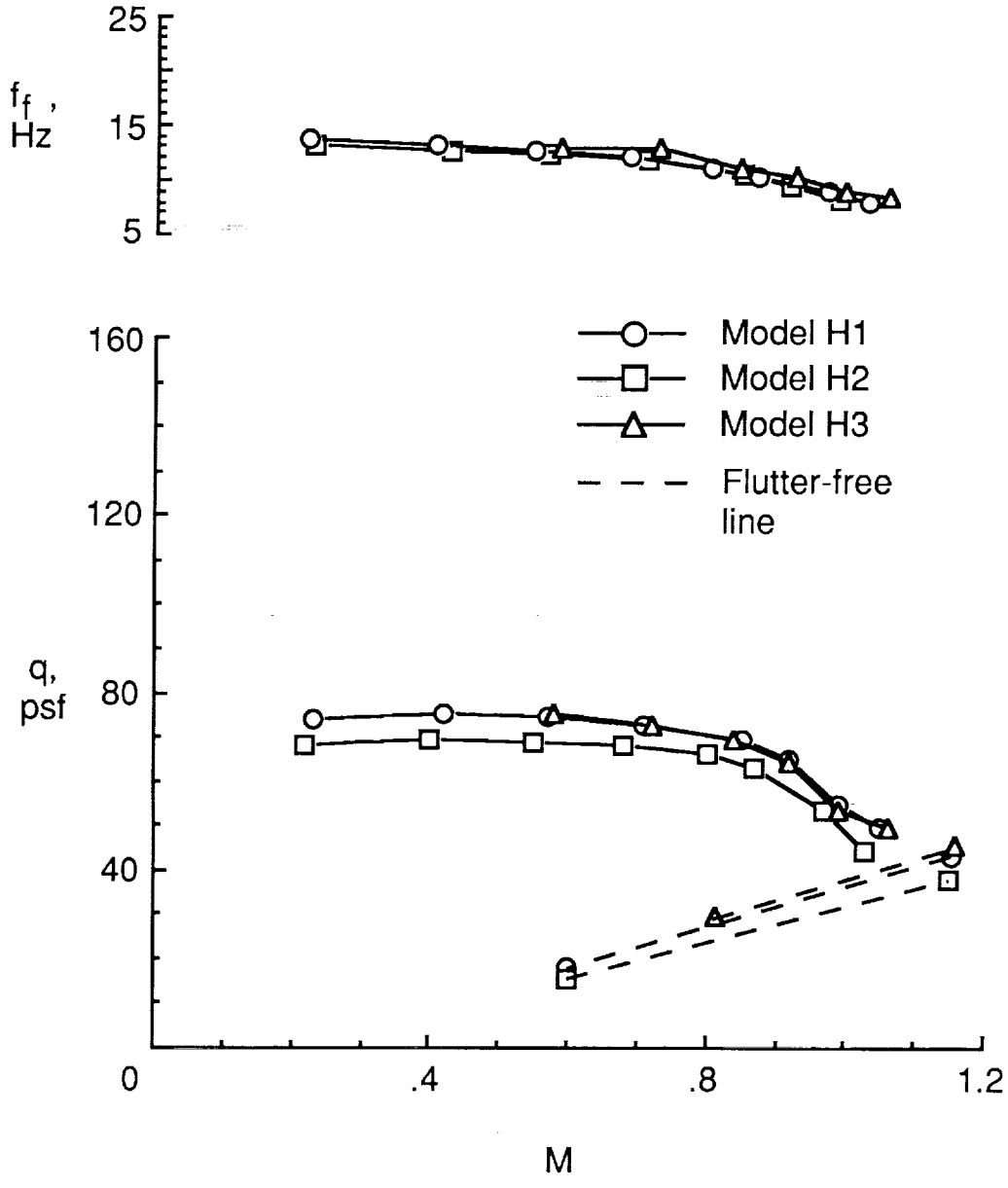

Figure 5. Flutter characteristics of H-series models in air.

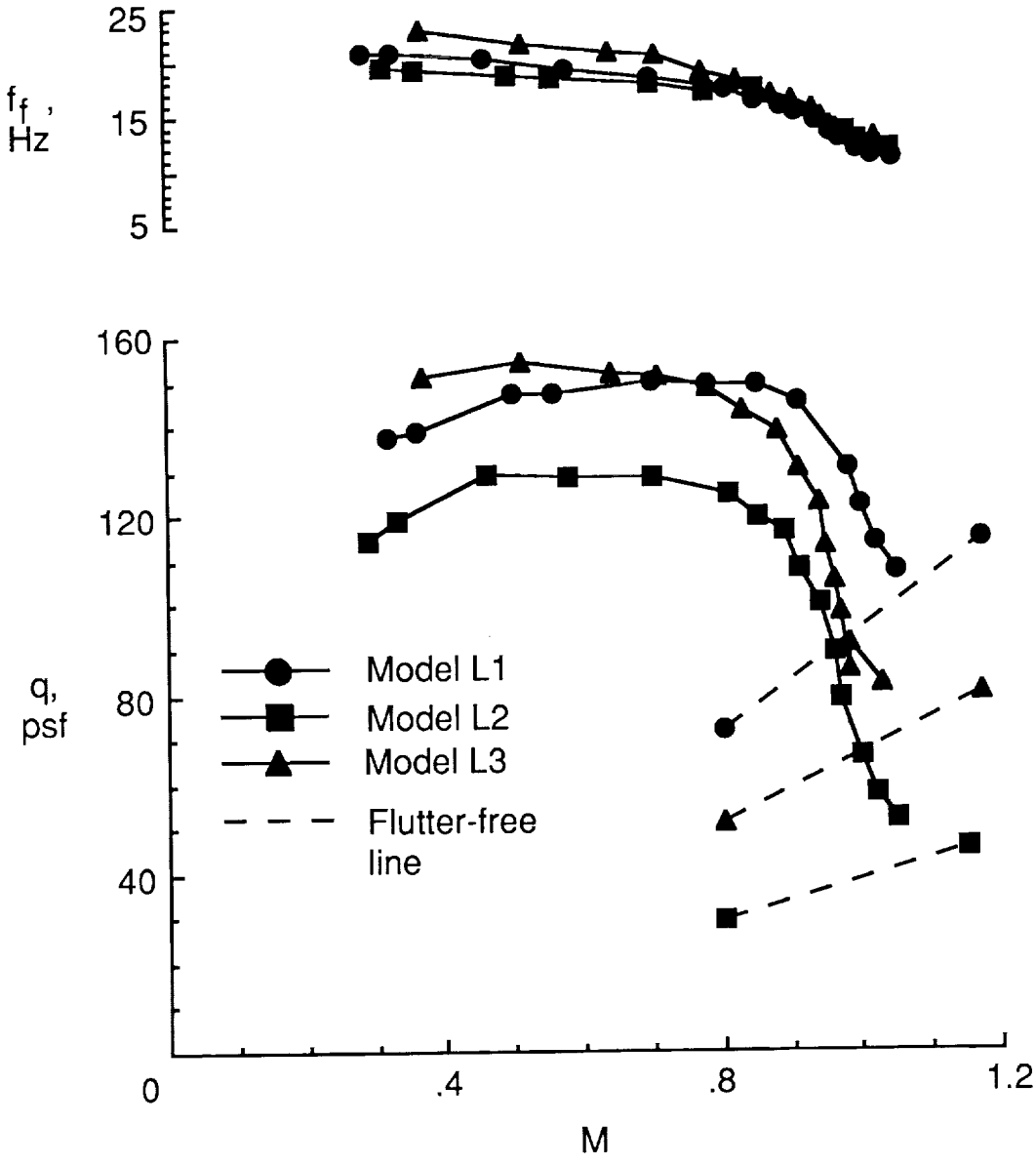

Figure 6. Flutter characteristics of L-series models in air.

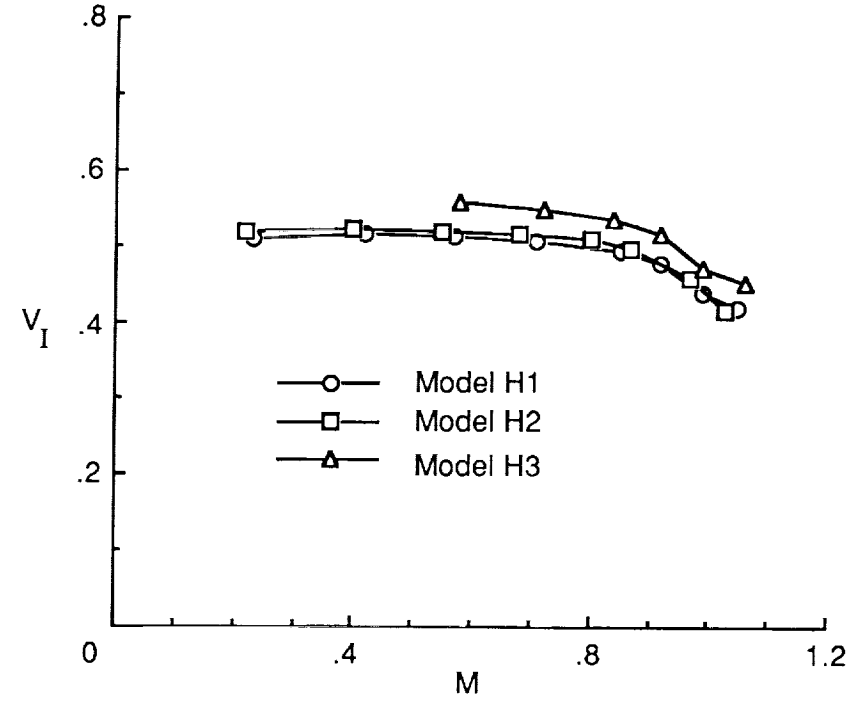

Figure 7. Nondimensional flutter characteristics of H-series models.

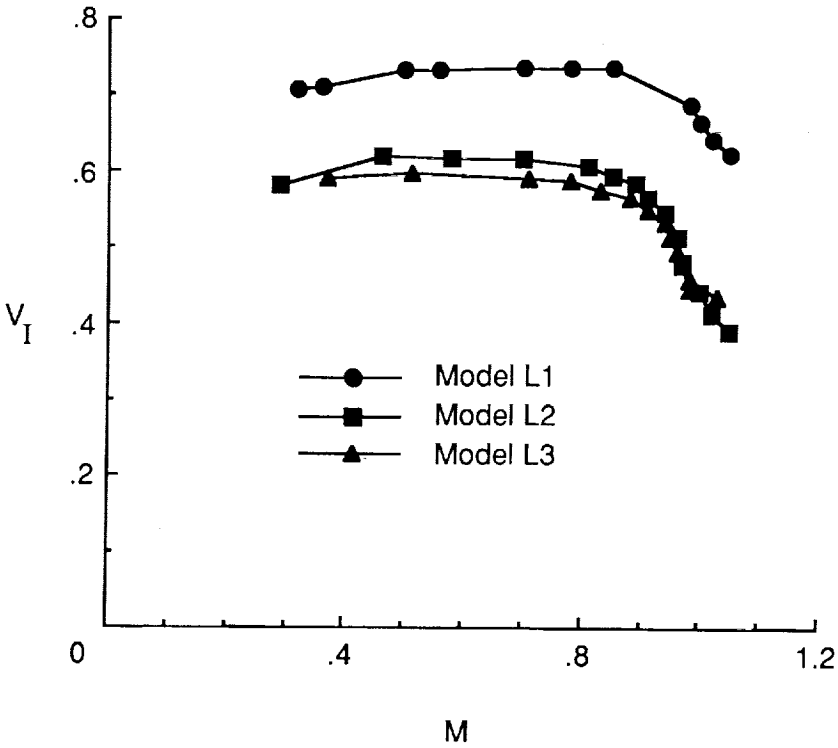

Figure 8. Nondimensional flutter characteristics of L-series models.

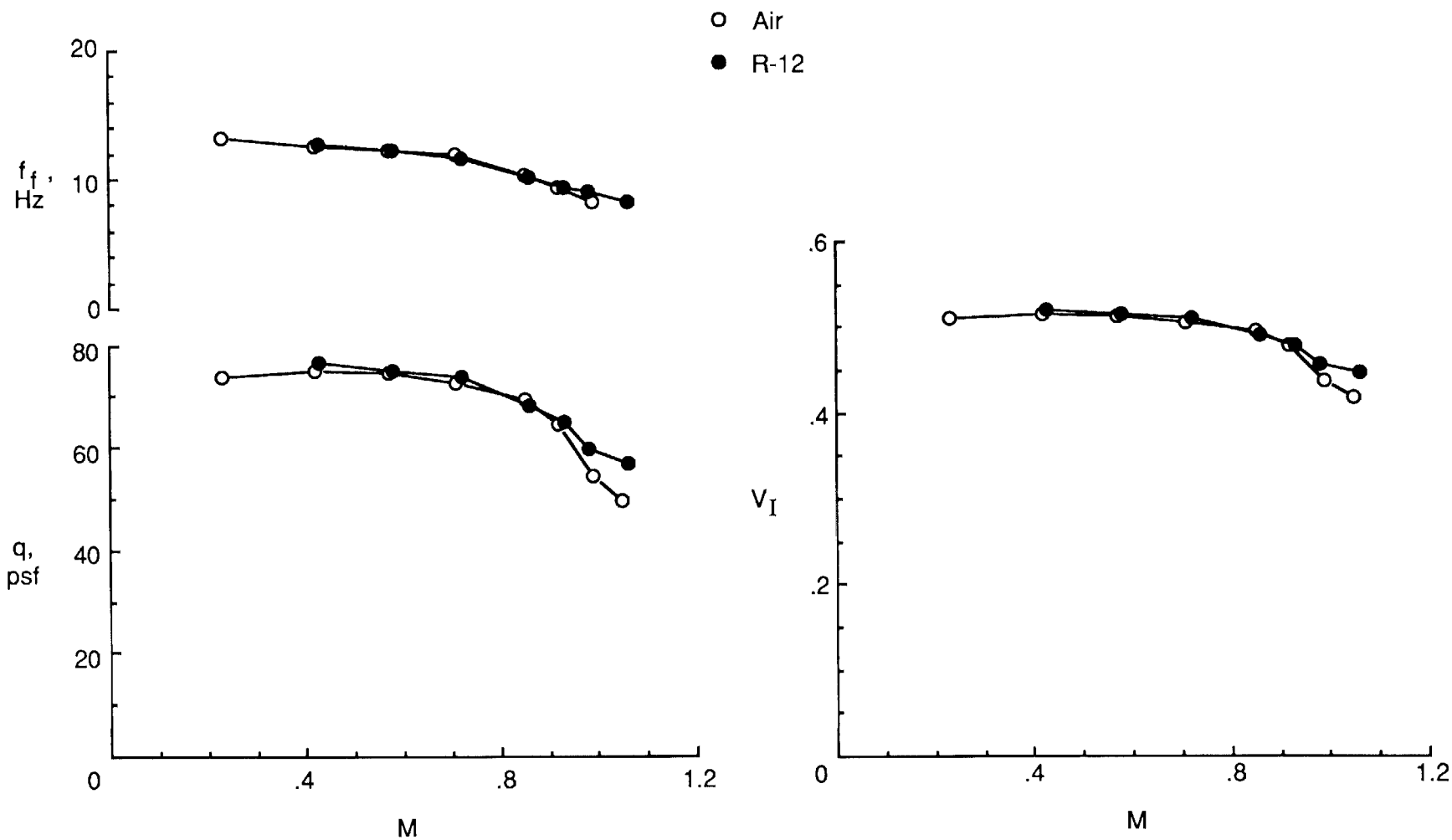

Figure 9. Flutter characteristics of model H1 in air and R-12.

NASA
National Aeronautics and Space Administration

Report Documentation Page

1. Report No.	2. Government Accession No.	3. Recipient's Catalog No.
NASA TM-4180		

4. Title and Subtitle
An Experimental Study of Tip Shape Effects on the Flutter of Aft-Swept, Flat-Plate Wings

5. Report Date
June 1990

6. Performing Organization Code

7. Author(s)
Bryan E. Dansberry, José A. Rivera, Jr., and Moses G. Farmer

8. Performing Organization Report No.
L-16638

9. Performing Organization Name and Address
NASA Langley Research Center
Hampton, VA 23665-5225

10. Work Unit No.
505-63-21-09

11. Contract or Grant No.

12. Sponsoring Agency Name and Address
National Aeronautics and Space Administration
Washington, DC 20546-0001

13. Type of Report and Period Covered
Technical Memorandum

14. Sponsoring Agency Code

15. Supplementary Notes

16. Abstract

The effects of tip-chord orientation on wing flutter are investigated experimentally using six cantilever-mounted, flat-plate wing models. Experimentally determined flutter characteristics of the six models are presented for both subsonic and transonic Mach number ranges. While all models have a 60° leading-edge sweep, a 40.97° trailing-edge sweep, and a root chord of 34.75 in., they are subdivided into two series characterized by a higher aspect ratio and a lower aspect ratio. Each series is made up of three models with tip-chord orientations that are parallel to the free-stream flow, perpendicular to the model midchord line, and perpendicular to the free-stream flow. Although planform characteristics within each series of models are held constant, structural characteristics such as mode shapes and natural frequencies are allowed to vary.

17. Key Words (Suggested by Authors(s))
Aeroelasticity
Flutter
Aft-swept wings
Tapered wings
Wingtip geometry
Low aspect ratio
Transonic
Zero angle of attack
Flat-plate model
Wind-tunnel test

18. Distribution Statement
Unclassified—Unlimited

Subject Category 05

19. Security Classif. (of this report)	20. Security Classif. (of this page)	21. No. of Pages	22. Price
Unclassified	Unclassified	20	A03

NASA FORM 1626 OCT 86

NASA-Langley, 1990

For sale by the National Technical Information Service, Springfield, Virginia 22161-2171